



# Influence of blade vibrations on aerodynamic performance of axial compressor in gas turbine: Direct numerical simulation



M.E. Nakhchi<sup>\*</sup>, S. Win Naung, M. Rahmati

Faculty of Engineering and Environment, Northumbria University, Newcastle Upon Tyne, NE1 8ST, UK

## ARTICLE INFO

### Article history:

Received 26 July 2021

Received in revised form

25 November 2021

Accepted 20 December 2021

Available online 22 December 2021

### Keywords:

Blade oscillations

Compressor

DNS

Spectral-hp element

Transient flow

## ABSTRACT

Flutter instability because of the blade vibrations is a major problem in axial compressor cascades. This paper investigates the effects of blade oscillations on aerodynamic performance and turbulent flow characteristics of modern gas-turbine compressors. Highly accurate direct numerical simulations (DNS) are performed based on the spectral-hp element method to predict the flow instabilities, pressure fluctuations and vortex generation on the surface of the compressor blades by considering all complex physical parameters at different vibration frequencies ( $0 < f < 8.28$  Hz). The main novelty of this study is to consider the aeroelastic vibrations of the compressor blades in DNS analysis. The novel proposed method enables the detailed analysis of complex structure fluid interactions, which cannot be obtained using other methods such as RANS models. The simulations revealed that the blade oscillations have a huge impact on the vortex generation and laminar separation bubble on the suction side of the blade. Moreover, the amplitude of unsteady pressure distribution is greater at 90% span, with the phase angle deviating between  $100^\circ$  and  $350^\circ$ . Strong fluctuations are observed at the centre of the wake region of the vibrating blade cascade. These fluctuations are activated by the flow disturbances resulting from the blade oscillation. Moreover, intense pressure fluctuations happen in the wake region of the oscillating compressor blade compared with the stationary one. The separating point occurred 8.28% sooner on the suction surface of the vibrating blade with  $k = 0.4$  ( $X_{sep}/C = 0.288$ ) compared to the stationary blade with  $X_{sep}/C = 0.314$ .

© 2022 The Authors. Published by Elsevier Ltd. This is an open access article under the CC BY license (<http://creativecommons.org/licenses/by/4.0/>).

## 1. Introduction

In the past decade, with increasing energy demands, there has been increased competition in improving performance while decreasing the weight of the power energy production systems such as wind or gas turbines [1,2]. Gas turbines can produce a huge amount of electrical power energy on a small-scale power plant [3]. The axial compressors blades in gas turbines are subject to aeroelastic instabilities inducing blades vibrations [4]. The improvement in the performance of the gas turbines can be achieved when the complex fluid-structure interaction is considered. The blades aeroelastic oscillations have a noticeable impact on vortex generation and flow separation point on the surface of the compressor blades. These vibrations usually cause damage to turbine blades due to unpredicted flutter instabilities and pressure fluctuations on the surface of the compressor blades. Developing a high-fidelity

transient numerical method is vital to accurately capture the flow behaviour on the blade surface under transitional flow regimes. This is especially crucial for advanced aircraft gas turbine compressors, which are made of light-weight aerofoils, and the flutter prediction is essential in the design of these compressor blade cascades.

Aeroelastic analysis of the compressor blades in gas turbine engines is a key concern for turbomachinery designers. Flutter instabilities because of the blade's vibrations become a noticeable problem in the compressor cascade and also in the low-pressure turbines [5]. Therefore, providing a more realistic analysis will help to better understand and calculate the blades flutter instabilities and unsteady flow behaviour on the compressor blades at various air speeds. This challenge has become a major focus by researchers in the past decade because the aeroelastic mechanism is complex, and several parameters impact the details of the flow structure, separating point and oscillations of the compressor blade cascade.

The rotation of nearby blades in compressor cascade in aircraft

<sup>\*</sup> Corresponding author.

E-mail address: [mahdi.nakhchi@northumbria.ac.uk](mailto:mahdi.nakhchi@northumbria.ac.uk) (M.E. Nakhchi).

**Nomenclatures**

$A$	Vibration amplitude, m
$C$	Blade chord length, m
$C_{p1}$	Unsteady pressure coefficient
$f$	Vibration frequency, Hz
$h$	Blade span, m
$k$	Reduced vibration frequency
$L_z$	Span length
$N_p$	Planes in span direction
$p$	Pressure, Pa
$Re$	Reynolds number
$S_0$	Step function
$\mathbf{u}$	Velocity vector
$W_z$	Span vorticity

*Greek symbols*

$\beta$	Inflow angle
$\omega$	Oscillation function
$\Omega$	Computational domain
$\varphi$	Mapping function

engines generates transient turbulent flow perturbations and vortex generations, which have an unfavourable impact on the noise transmission and flutter instabilities [6]. In the advanced compressors in gas turbines, these complex flow unsteadiness and separation point predictions play important roles in the design of blade rows. The aeroelastic oscillations of the linear compressor cascade blades have a noticeable impact on the pressure coefficient and flow separation compared to the stationary blades without vibrations. However, the effects of the aeroelastic vibrations of the compressor blades with high-fidelity methods have not been investigated yet. So, it is essential to perform a highly accurate numerical simulation over the compressor blades in gas turbines by considering all complex physical parameters and the realistic oscillating behaviour of the blade rows.

Several numerical and experimental turbomachinery studies have been conducted in the past decade to investigate the flutter instabilities over the compressor cascade and turbine blades in modern gas turbines. Yang and He [7] performed an experimental study on linear compressor cascade by considering the blade vibrations. They observed that the flow structure is fully three-dimensional and unsteady. Their conclusions indicated that performing a transient flow simulation is important to precisely detect flow instabilities in a linear compressor blade due to blade vibration. They also found that the overall aerodynamic damping was reduced by 27% by increasing the tip gap from 0% to 2%. Rahmati et al. [8] developed the nonlinear frequency-domain method to numerically investigate the aerodamping and pressure variations on the suction side and pressure side of the multistage turbine blades. They found that the newly proposed model has good agreement with the well-known time-domain method with a significant reduction in the computation time. Shine et al. [9,10] numerically investigated the aeroelastic behaviour of the wind turbine blades. The simulations showed that the frequency-domain methodology is able to evaluate the transient flow details and the pressure coefficient on the turbine blades with higher precision in comparison with Reynolds-averaged Navier-Stokes (RANS) models. However, the main focus of these studies is to precisely predict the aeroelastic behaviour and aeroelasticity parameter known as aerodynamic damping. Further investigations on the flow details including vorticity structures are required in order to improve

physical understandings in compressors, especially when the blade vibrations are involved.

Reynolds-averaged Navier-Stokes models are typically used to predict flow behaviour of turbine blades. The effects of geometric variations on the aerodynamic performances of a low-pressure turbine blade were analysed by Wang et al. [11], employing a RANS model for the aerodynamic computation. Du et al. [12] numerically and experimentally optimised the performance of industrial high loaded gas compressors by providing flow control mechanisms such as Coanda jets. They used RANS model for the numerical aerodynamic simulations over the compressor blade. They found that the static pressure coefficient can be enhanced by 8.8% when the mass flow rate of the jet is 1.5%. The effects of the blade's corrosion on the aerodynamic performance of gas turbines were investigated by Yonezawa et al. [13]. They used the RANS model based on the finite volume method to perform their numerical simulations on the gas turbine blade. It was concluded that the corrosion on the surface of the blade has a noticeable impact on the isentropic efficiency of the turbine. Furthermore, Shuai et al. [14] performed an experimental and numerical investigation of the effect of bending clearance of a blade tip region of a linear turbine cascade on the aerodynamic performances. A RANS model is employed for their numerical investigation. Abolfazl Moussavi et al. [15] experimentally and numerically investigated the impacts of splitter leading edge on the performance improvement of turbo-charger compressors. They concluded that shorter splitter compressor blades with an inclined leading edge could enhance the compressor's efficiency.

Furthermore, RANS models are also found in the aeroelasticity analysis of the turbomachinery applications. Zhang et al. [16] employed the RANS method to perform simulations over a wind turbine under stalled flow conditions. They found that the Strouhal number measuring the transient vortex shedding was in the range of 0.16–0.2 for different blade sections. Li and Liu [17] employed the RANS model to predict the flow structure and aerodynamic characteristics on the surface of NASA-Stage-35 blade. They simplified the governing equations by considering the ideal gas law. Alam et al. [18] numerically investigated the transition onset from laminar to turbulent flow regime on the wind turbine aerofoil. They found that the bubbles with turbulence reattachment generated the highest adverse pressure gradient. In the numerical simulations of Vahdati and Zhao [19], the authors employed the RANS model to investigate the fan blade flutter instabilities. They also detected the flutter stall details and separation occurrence due to the unsteady pressure fluctuations on the blades.

Low-fidelity and simplified turbulent models cannot accurately predict the details of the transitional mechanism and fluid-structure interaction due to the aeroelastic vibrations. As discussed earlier, previous studies were mainly based on low-fidelity numerical methods, such as RANS method. Recently, turbomachinery researchers were focused on performing direct numerical simulations (DNS), large-eddy simulations (LES) or other newly proposed high-fidelity transient models instead of the conventional RANS models over the turbines and compressor blades. Win Naung et al. [20] performed DNS to analyse the interface between the transitional flow and the vibrating turbine blades. It was found that the DNS can predict the pressure coefficient on the blade surface more accurately. Nakhchi and Rahmati [21] performed DNS over the vibrating turbine blades with different vibration frequencies ( $f = 0, 5.2$  Hz and  $10.3$  Hz). They found that the flow separation on the suction side of the non-oscillating blades happens at  $S_{sep}/S = 0.391$ , while it happens at  $0.372$  over the oscillating blades with  $f = 5.2$  Hz. The simulations revealed that the vibrations have a significant impact on the flow disturbance and vortex generation on the surface of the blade. Moriguchi et al. [22] employed a

high-order finite element based LES model to investigate the aerodynamic performances of a linear turbine cascade. However, their analysis is based on a stationary blade and the unsteady effects due to blade elasticity are completely ignored. Nakhchi et al. [23] performed DNS over the NACA airfoils at a wide range of design parameters to predict the flutter instabilities over the wind turbine blades under realistic flow conditions. It was revealed that increasing the Reynolds number makes the vortex generation stronger and increases the pressure fluctuations on the airfoil surface. The separation point occurred faster from  $S_{sep}/S = 0.58$  to 0.19 by increasing the angle of attacks from  $16^\circ$  to  $0^\circ$ . D'Alessandro et al. [24] performed unsteady numerical simulations by using LES to control the separated shear layer and stall on dimpled turbine blades with NACA aerofoil. It was concluded that the dimpled surface reduced laminar separation bubble (LSB) size if the dimples were placed before the separation point.

The spectral-hp element method as a powerful high-order and precise numerical method is grown rapidly in the past few years [25]. This direct numerical simulation (DNS) method can predict the instantaneous aerodynamic flow structure, flow detachment and reattachment, LSB and pressure coefficient over different geometries. The main benefit of this newly proposed method compared to other DNS techniques is that this method is much more computational efficient over three-dimensional bodies, which make it more applicable to be employed over wind turbine blades. This method can predict the aerodynamic characteristics at a wide range of Reynolds numbers [26] by using both incompressible [27] and compressible solvers [28]. It means that this method can be used to simulate the flow over oscillating HAWTs at lower Reynolds numbers. The study of Moxey et al. [29] revealed that the open-source code NEKTAR++, which is designed according to the spectral-hp element method, is improved significantly in the past two years. Moreover, this method provides the ability to simulate the laminar/turbulent flows by considering the vibrations of the bodies. The numerical study of Bao et al. [30] revealed that the vibrations could change the pressure coefficient and recirculation flows over the cylindrical risers. They used the spectral-hp element method for DNS computations. Cassinelli et al. [31] employed this DNS technique to investigate the turbulent flow structure and wake profile on a stationary low-pressure turbine (LPT). As discussed earlier, nearly all the previous numerical simulations over oscillating wind turbine blades were two-dimensional. Only one recent study used three-dimensional wind turbine airfoil to investigate the flow separation over the blades. However, they used URANS method which cannot precisely predict the transitional flow regime and instantaneous vorticity contours over the turbine blade.

Based on the above literature review, accurate prediction of aeroelastic performance and details of the flow separation on the oscillating compressor blades in modern gas turbines remains an unresolved and challenging problem for gas turbine designers. Moreover, previous simulations in the field of compressors were mostly conducted on stationary blades using low-fidelity RANS models. The effects of the aeroelastic vibrations of the compressor blades are yet to be thoroughly investigated. The main novelty of this study is to consider the aeroelastic vibrations of the compressor blades by developing a high-fidelity DNS model to predict the flutter instability, vortex generation and time-dependent variations of the pressure fluctuations on the surface of compressor blades. In this study, the spectral-hp element high-order method is employed for the first time to investigate the transient aerodynamic characteristics of the compressor blade cascade by considering all complex physical parameters and the realistic oscillating behaviour of the blade rows. The flow is turbulent, and the blades oscillate with specific vibration frequencies.

For the first time, the details of the vortex generation and pressure coefficient on the surface of a stationary compressor blade are compared with a stationary one at specific Reynolds numbers. The effects of the vibrations on the flow instabilities, axial velocity contours, and the wake profile are also investigated. The proposed simulation method in this study will help designers to improve the efficiency and life expectancy of the compressor blades and predict the flutter instabilities under complex and time-dependent blade oscillations.

## 2. Physical model

The details of the linear compressor cascade with the inflow conditions are shown in Fig. 1. For validation and comparison purposes, the geometry of the linear compressor cascade is designed based on the benchmark study of Elazar and Shreeve [32] for a non-oscillating modern gas-turbine compressor blade. In the present numerical study, two different Reynolds numbers of  $1.95 \times 10^5$  and  $7 \times 10^5$  are selected for the DNS simulations over the stationary and vibrating compressor cascades. The Reynolds number is defined based on the inflow velocity and the chord length ( $Re = \frac{U_\infty C}{\nu}$ ) of the blade. The inflow angle ( $\beta$ ) is  $37.5^\circ$ . The blade oscillates in the normal direction with a sinusoidal function of  $y = A \sin(\omega t)$ , where  $A$  is the vibration amplitude and  $\omega = 2\pi f$  is the vibration frequency. The vibration frequencies ( $f = 4.14, 8.28$  Hz) are selected based on the experimental study of Yang and He [7], which are popular in realistic low-speed gas turbine engines. The details of the aerodynamic forces on the compressor airfoil and the definition of the lift and drag parameters are provided in Fig. 2. The geometrical parameters of the compressor blade are shown in Table 1.

## 3. Numerical methodology

The time-dependent and incompressible Navier-Stokes equation in the vector type in a three-dimensional model can be expressed as:

$$\partial_t \mathbf{u} + (\mathbf{u} \cdot \nabla) \mathbf{u} = -\nabla p + \nu \nabla^2 \mathbf{u} \quad (1)$$

$$\nabla \cdot \mathbf{u} = 0 \quad (2)$$

where  $\mathbf{u}$ ,  $p$  and  $\nu$  are the velocity vector ( $u, v, w$ ), pressure, and kinematic viscosity of air. The simulations were extended in span direction (third dimension) by using Fast Fourier Transform in spectral-hp element solver. As discussed in the literature review, this method can detect the instantaneous turbulent flow characteristics by considering the compressor cascade oscillations at different

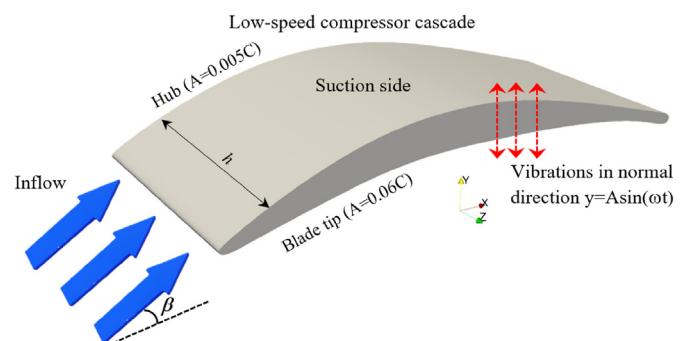


Fig. 1. Schematic view of the oscillating linear compressor blade.

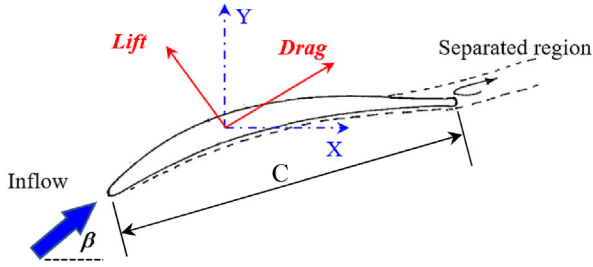


Fig. 2. Force diagram and flow direction over a vibrating compressor airfoil.

**Table 1**  
Design parameters of the compressor cascade in modern gas turbine.

Item	Description
Blade type	Controlled diffusion gas-turbine airfoil
Chord length, $C$	0.15 m
Span length, $h$	0.19 m
Aspect ratio, $h/C$	1.27
Maximum thickness	0.07C
Leading edge radius	0.00132 m
Trailing edge radius	0.00186 m
Vibration direction	Normal to the blade chord
Vibration amplitude at tip, $A_{tip}$	0.06C
Vibration amplitude at hub, $A_{hub}$	0.005C
Vibration function	$Y = A \sin(\omega t)$ , $\omega = 2\pi f$
Vibration frequency, $f$	4.14, 8.28 Hz
Reduced frequency, $k$	0.2, 0.4
Inflow angle, $\beta$	37.5°
Inflow Reynolds number, Re	$1.95 \times 10^5$ , $7 \times 10^5$

inlet velocities. This method utilises a moving reference frame to add vibrations to the airfoil body surface. The latest version of NEKTAR++ code (V5.0.2) was used for the DNS simulations on the ARCHER2-UK HPC cluster by using parallel processing with 256 dual AMD Rome 64 core CPUs at 2.2 GHz and 128 GB of Memory.

Similar to other finite element methods, the spectral-hp element method works with domain decomposition into sub-domains such  $\Omega = \cup_{e \in \mathcal{E}} \Omega_e$ . In which  $\Omega$  is the total computation domain and  $\Omega_e$  is the sub elements in physical space. The spectral-hp element method uses mapping functions to convert the local cartesian geometry  $(x_1, x_2)$  into a reference coordinate system of  $(\xi_1, \xi_2)$  in the mapped space such that:

$$x_1 = \chi_1^e(\xi_1, \xi_2), \quad x_2 = \chi_2^e(\xi_1, \xi_2) \quad (3)$$

More details of the domain decomposition and mapping methodology are discussed in Ref. [33]. The cartesian structure can describe the mapping function in the spatial domain as tensorial spectral-hp element expansions as [34]:

$$u(\xi_1, \xi_2) = \sum_{n \in \mathbb{N}} \varphi_n(\xi_1, \xi_2) \hat{u}_n = \sum_{p=0}^P \sum_{q=0}^P \psi_p(\xi_1) \psi_q(\xi_2) \hat{u}_{pq} \quad (4)$$

Where  $\varphi_n$  is a two-dimensional function that can be expressed as a tensor product of a one-dimensional function of  $\psi_p$ .

This spectral-hp element method is based on various schemes to simulate incompressible and/or compressible flows. In the current DNS study, the continuous Galerkin (CG) method is chosen for the analysis of the compressor aerofoil. The momentum equation (Eq. (1)) could be expressed as:

$$\partial_t \mathbf{u} = N(\mathbf{u}) - \nabla p + \nu \mathcal{L}(\mathbf{u}) \quad (5)$$

In the above equation,  $N(u) = u(u \cdot \nabla)$  and  $\mathcal{L}(u) = \nabla^2 u$  are the non-linear and linear convective and diffusive terms of the Navier-

Stokes equation, respectively. According to the velocity-correction scheme, the advection term can be expressed as:

$$\mathbf{u}^* = - \sum_{q=1}^J \alpha_q \mathbf{u}^{n-q} - \Delta t \sum_{q=0}^{J-1} \beta_q N(\mathbf{u}^{n-q}) \quad (6)$$

The Poisson and Helmholtz terms in the solver flowchart (Fig. 3) can also be defined as:

$$\nabla^2 p^{n+1} = \frac{1}{\Delta t} \nabla \cdot \mathbf{u}^* \quad (7)$$

$$\nabla^2 \mathbf{u}^{n+1} - \frac{\alpha_0}{\nu \Delta t} \mathbf{u}^{n+1} = - \frac{\mathbf{u}^*}{\nu \Delta t} + \frac{1}{\nu} \nabla p^{n+1} \quad (8)$$

By performing time-integration on the momentum equation and using the above expressions for the advection, Poisson and Helmholtz terms, the momentum equation in  $n+1$ st time-step can be discretised as follows [23]:

$$\frac{\gamma_0 \mathbf{u}^{n+1} - \sum_{q=0}^{J_i-1} \alpha_q \mathbf{u}^{n-q}}{\Delta t} = \sum_{q=0}^{J_e-1} \beta_q N(\mathbf{u}^{n-q}) - \nabla p^{n+1} + \nu \mathcal{L}(\mathbf{u}^{n+1}) \quad (9)$$

In which  $J_e$  and  $J_i$  are the explicit and implicit terms. Eq. (9) may be expressed as:

$$\frac{\gamma_0 \mathbf{u}^{n+1} - \mathbf{u}^+}{\Delta t} = N^+ - \nabla p^{n+1} + \nu \mathcal{L}(\mathbf{u}^{n+1}) \quad (10)$$

In which  $\mathbf{u}^+ = \sum_{q=0}^{J_i-1} \alpha_q \mathbf{u}^{n-q}$  and  $N^+ = \sum_{q=0}^{J_e-1} \beta_q N(\mathbf{u}^{n-q})$ . By performing integration over the computational field  $\Omega$ , the weak form of the Poisson equation can be expressed as:

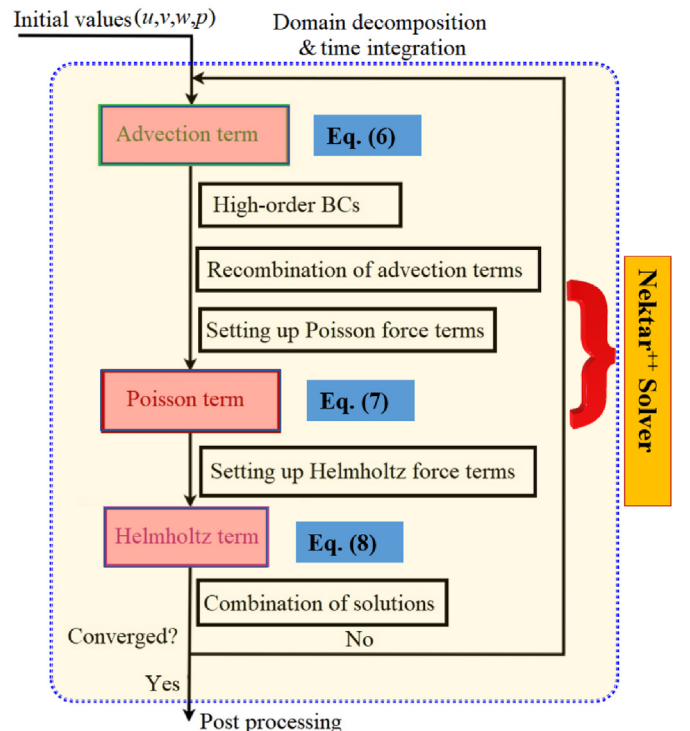


Fig. 3. Spectral-hp element method solution algorithm.

$$\int_{\Omega} \nabla p^{n+1} \cdot \nabla \varphi d\Omega = \int_{\Omega} \left[ \frac{\mathbf{u}^+ - \gamma_0 \tilde{\mathbf{u}}^{n+1}}{\Delta t} + N^+ - \nu(\nabla \times \nabla \times \mathbf{u})^* \right] \cdot \nabla \varphi d\Omega \quad (11)$$

In the above equation,  $\nabla \varphi$  is an operating function over the computational domain. After computing the above equations, finally,  $\mathbf{u}$  can be evaluated by Ref. [27]:

$$\mathbf{u}^{\delta}(\xi, t) = \sum_n \hat{u}_n \varphi_n(\xi, t) \quad (12)$$

The aim is to compute the terms of  $\hat{u}_n$ . At the outlet of the domain, a high-order outflow boundary condition was employed to accurately predict the vorticities and recirculations at the outlet. The following equation was employed to evaluate the Dirichlet outflow pressure:

$$p^{n+1} = \nu \mathbf{n} \cdot \nabla \cdot \mathbf{u}^{*,n+1} \cdot \mathbf{n} - \frac{1}{2} \left| \mathbf{u}^{*,n+1} \right|^2 S_0(\mathbf{n} \cdot \mathbf{u}^{*,n+1}) + f_b^{n+1} \cdot \mathbf{n} \quad (13)$$

Where  $S_0(\mathbf{n} \cdot \mathbf{u}) = \frac{1}{2} \left( 1 - \tanh \frac{\mathbf{n} \cdot \mathbf{u}}{u_0 \delta} \right)$  is a step function,  $u_0$  denotes the characteristics velocity, and  $\delta$  is a non-dimensional positive constant [35]. The following equation is used to compute the velocity components as:

$$\nabla \mathbf{u}^{n+1} \cdot \mathbf{n} = \frac{1}{\nu} \left[ p^{n+1} \mathbf{n} + \frac{1}{2} \left| \mathbf{u}^{*,n+1} \right|^2 S_0(\mathbf{n} \cdot \mathbf{u}^{*,n+1}) - \nu (\nabla \cdot \mathbf{u}^{*,n+1}) \mathbf{n} - f_b^{n+1} \right] \quad (14)$$

The details of the solver algorithm based on the Continuous Galerkin (CG) scheme in the spectral-hp element method are presented in Fig. 3.

### 3.1. Mesh generation

Fig. 4 shows the details of the mesh generation for DNS simulations over the compressor cascade. For better presentation of the grid, each element is divided into five sections ( $P = 5$ ) on the edges. To achieve highly accurate results and to detect the instantaneous flow instabilities on the surface of the compressor blade, the polynomial order must be higher. A grid independence study is necessary to find the most appropriate polynomial order for the DNS simulations. Eight inflated layers with the smallest size of 0.004 m for the adjacent layer with a growth rate of 1.2 is chosen to capture the boundary layer characteristics near the blade surface. A refined grid is utilised in the separated area on the suction side of the blade and also in the wake region to better capture the vortex generation in these regions. The grid is divided into 64 layers in the span direction ( $N_p = 64$ ), and the span length is set to be  $L_z = 0.4$ .

### 3.2. Grid independence study

To find the most appropriate polynomial order of the spectral-hp element method to achieve both required precision and avoiding unnecessary computational resources, it is necessary to perform a grid independence test. The dimensionless separation occurrence point ( $X_{sep}/C$ ) on the surface of the compressor in the gas turbine is computed at  $Re = 1.95 \times 10^5$  and  $\beta = 37.5^\circ$  to find the

required polynomial order ( $P$ ). The computed separation points for various polynomial orders are provided in Table 2. The simulations were performed for five different  $P$ -orders varying from 4 to 12. The deviations of the predicted separation point compared to the previous polynomial order are also provided. It is observed that the polynomial order of ten ( $P = 10$ ) can precisely predict the separation occurrence on the suction side of the blades at a specific Reynolds number and inflow angle. Consequently,  $P = 10$  is chosen for DNS computations on the linear compressor blade cascade in the gas turbine.

To resolve the viscous sub-layer near the surface of the compressor blades, inflated boundary layer mesh must be used near the walls. It is essential to use appropriate boundary-layer mesh with specific growth rates for DNS simulations with the spectral-hp element method. As discussed earlier, eight inflated layers with the smallest grid size of 0.004 m with a growth rate of 1.2 is employed to capture the vorticity generation and other important parameters on the suction side of the compressor blade. The following criteria must be met:  $\Delta x^+ < 20$ ,  $\Delta y^+ < 1$ , and  $\Delta z^+ < 10$  [36]. The “+” sign is the scale factor with the viscous length  $L^+ < \nu/u_\tau$  and  $u_\tau = \sqrt{\tau_w/\rho}$  is the frictional velocity. The computed values at  $Re = 1.95 \times 10^5$  and  $\beta = 37.5^\circ$  with  $P = 10$ ,  $L_z = 0.4$ ,  $N_p = 48$  on the surface of the compressor blades are shown in Fig. 5. The results show that the computed wall + values are in the acceptable range of the DNS analysis. Therefore, the boundary layer mesh is accurate enough to predict the vortex generation and flow disturbance near the walls of the oscillating linear compressor cascade.

## 4. Results and discussion

The results from the present DNS analysis are first compared to the experiment [7] for validation and to ensure its accuracy. Fig. 6 provides the comparison of the time-averaged pressure coefficient distribution over the blade surfaces at two different span sections between the present DNS simulation and the experiment. It is seen that the results from the present simulations are very close to the experimental data. An excellent agreement is also observed at different blade span sections.

The effects of the blade vibration on the vortex generation process are highlighted in comparison to the stationary blade. The vorticity isosurface from both stationary and oscillating blades are shown in Fig. 7. It is observed that the vortex generation is stronger in the latter case. The blade vibration causes the early flow separation compared to that of the stationary blade as the stagnation point is affected by the blade motion. The process is followed by the rolling up and recirculating of the separated shear layer on the suction side. In the case of the stationary blade, the vortex structures are smaller, and consistent vortex generation is detected over time. However, this process is influenced by the blade motion in the case of the vibrating blade as the dynamic stall vortex is observed with the larger vortex structures. These vortex structures break down when they leave the trailing edge, and the trailing edge vortex shedding is much stronger as a result of the blade oscillation in contrast to the stationary blade. The separation point occurred 8.28% sooner on the suction surface of the vibrating blade with  $k = 0.4$  ( $X_{sep}/C = 0.288$ ) compared to the stationary blade with  $X_{sep}/C = 0.314$ .

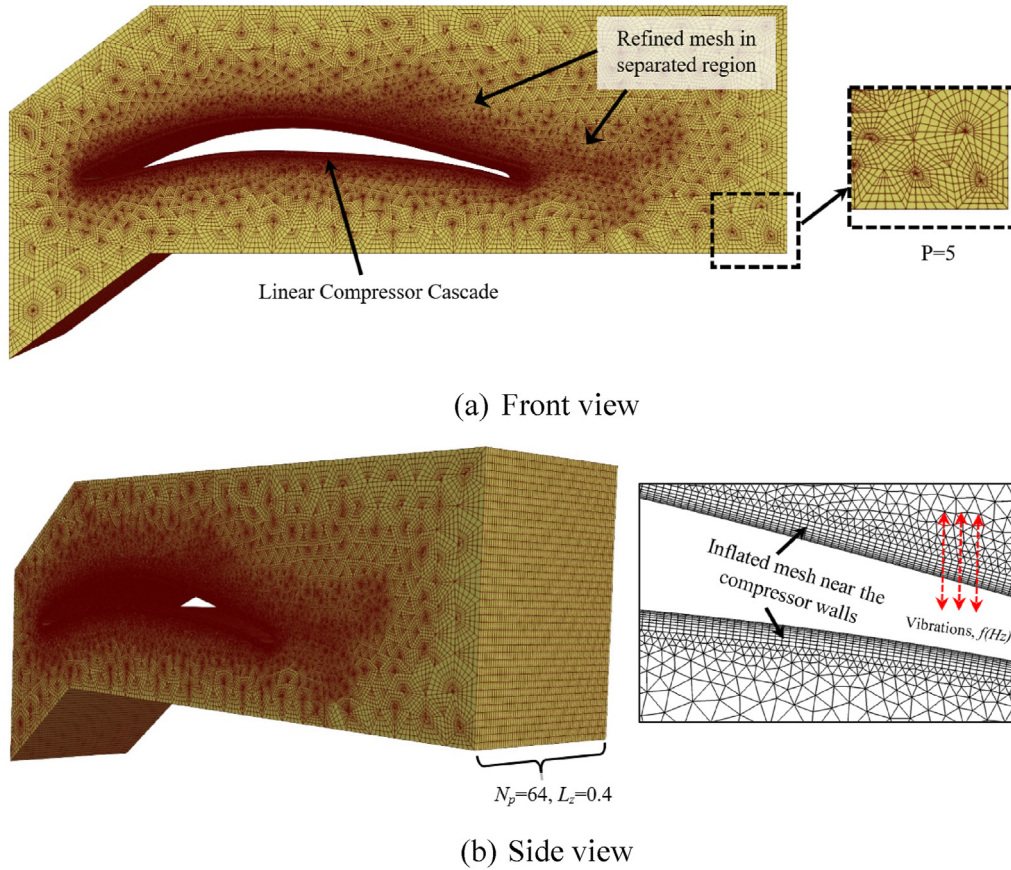


Fig. 4. Grid generation in the computational domain of linear compressor cascade with  $P = 5$ .

**Table 2**  
Grid independence study on the vibrating compressor cascade at  $Re = 1.95 \times 10^5$  and  $\beta = 37.5^\circ$ .

Polynomial order	$X_{sep}/C$	Deviation
$P = 4$	0.262	5.72%
$P = 6$	0.277	2.53%
$P = 8$	0.284	1.05%
$P = 10$	0.288	0.31%
$P = 12$	0.288	—

Unsteady pressure distributions over the blade pressure and suction sides, because of the blade oscillations, are also computed and compared to the experiment [7]. Unsteady pressure amplitude coefficient distributions are plotted in Fig. 8 at two blade sections for the reduced frequency of 0.4. It is found that the separation bubbles and the production of dynamic vortex flow resulting from the blade vibration have an impact on the pressure fluctuations on the suction side. The largest amplitude of fluctuation is found to be at around the leading edge of the blade, and the amplitude of pressure deviation is higher in the blade outer sections. At all sections of the blade, the results from the present DNS simulation are in good agreement with the experiment and the numerical results of the time-domain method [8]. It is observed that the DNS model used in this study predicts the pressure coefficient more accurately compared to the conventional time-domain method.

In the analysis of the aeroelasticity of turbomachinery, the distribution of unsteady pressure phase angle due to the blade motion is an important parameter and is also evaluated in this analysis. Fig. 9 demonstrates the comparison of the unsteady pressure phase

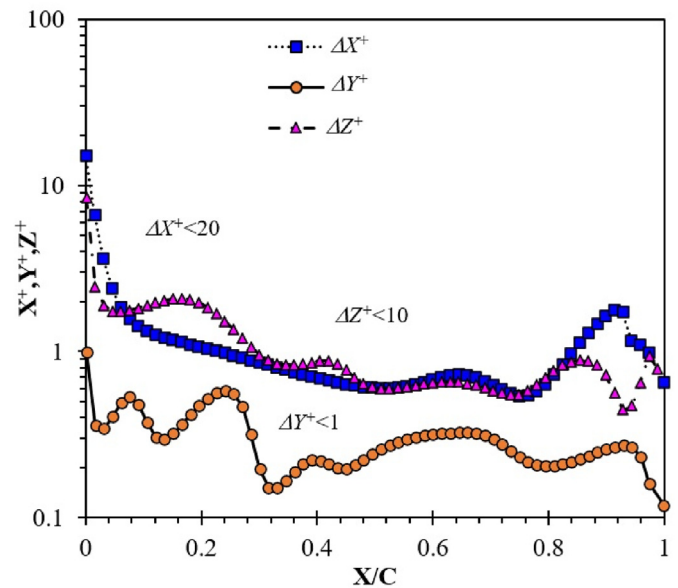


Fig. 5. Wall  $^+$  values for  $L_z = 0.4$  and  $N_p = 64$  at  $\beta = 37.5^\circ$  and  $Re = 1.95 \times 10^5$ .

angle computed from the present DNS simulation and the experimental results [7]. The results are extracted at 20% and 90% span sections at the reduced frequency of 0.4. As it is seen, the distribution of the unsteady pressure phase angle in the span direction is relatively small. This observation was also confirmed in the

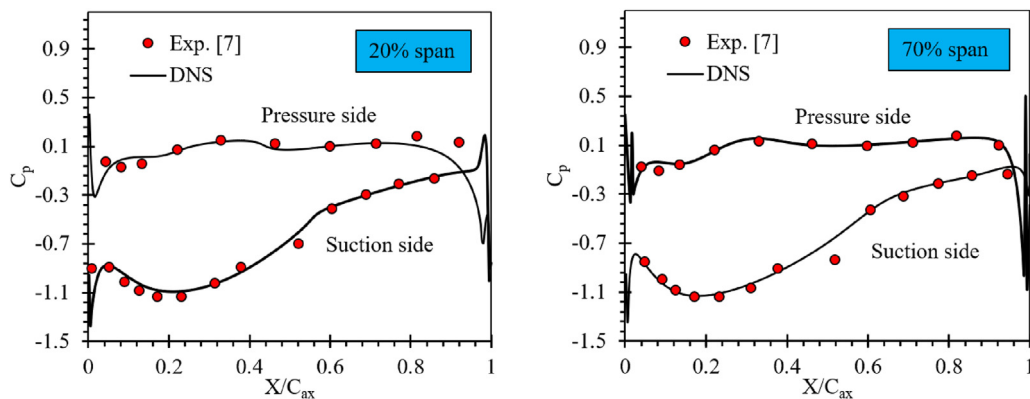


Fig. 6. Validation of the DNS results with experimental data [7] for  $C_p$  over the vibrating compressor.

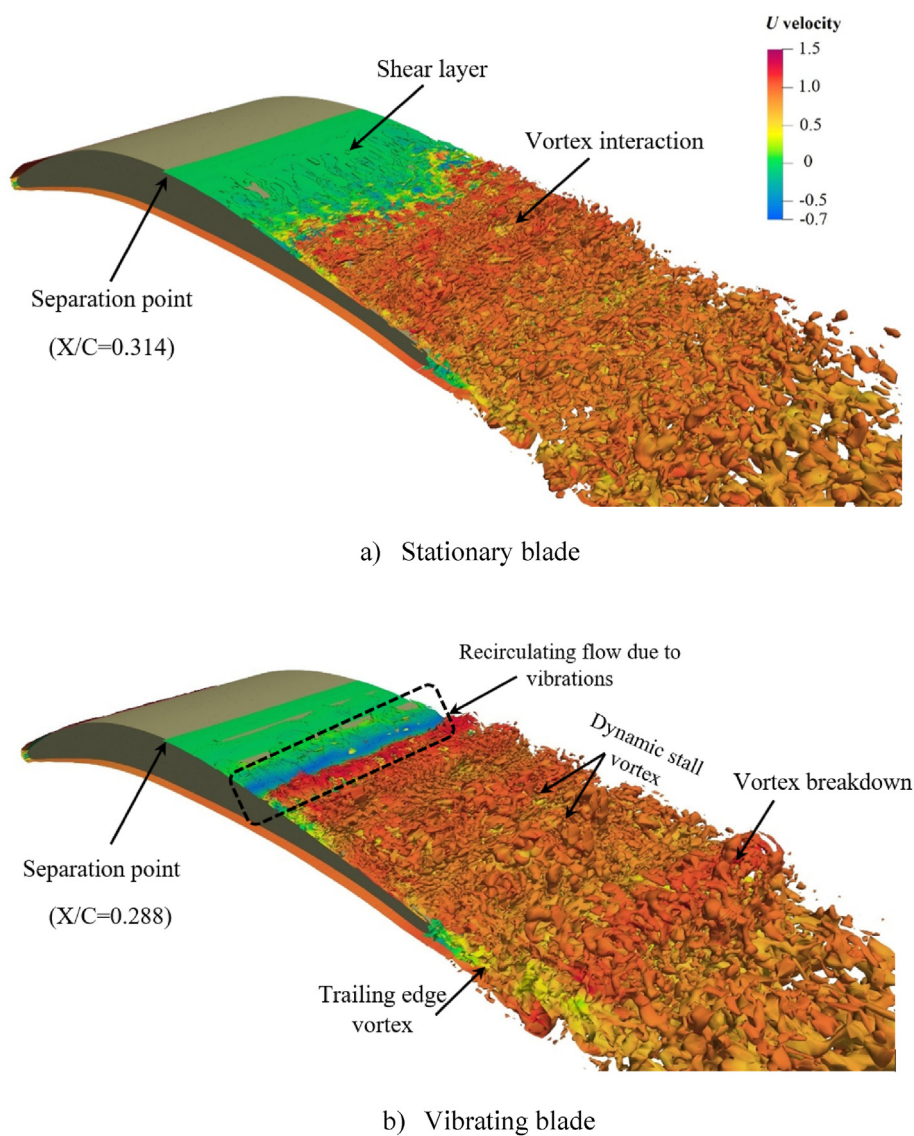


Fig. 7. Isosurface contours over the stationary and vibrating compressor cascade ( $k = 0.4$ ) at  $Re = 195,000$ .

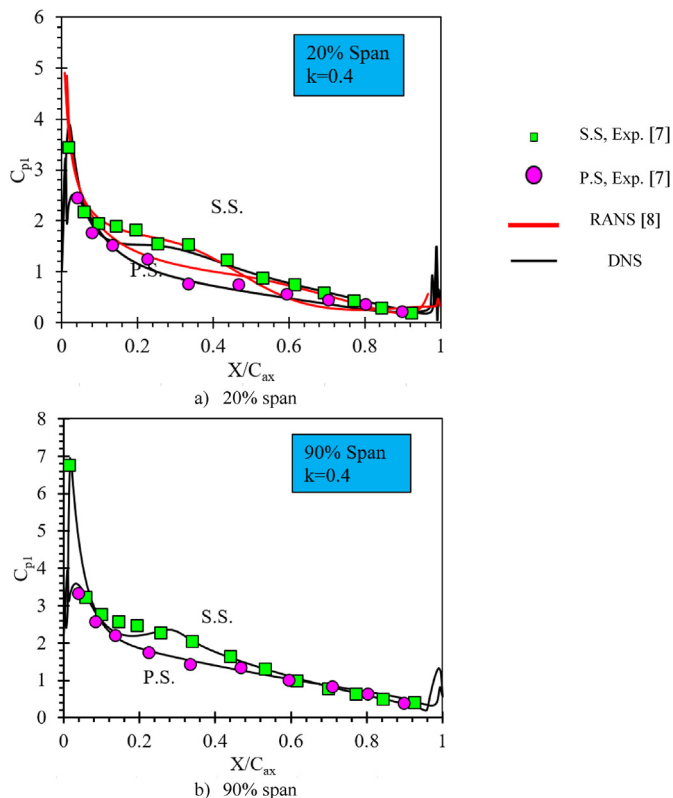


Fig. 8. Unsteady pressure coefficient over the vibrating compressor cascade ( $k = 0.4$ ) at two different span sections.

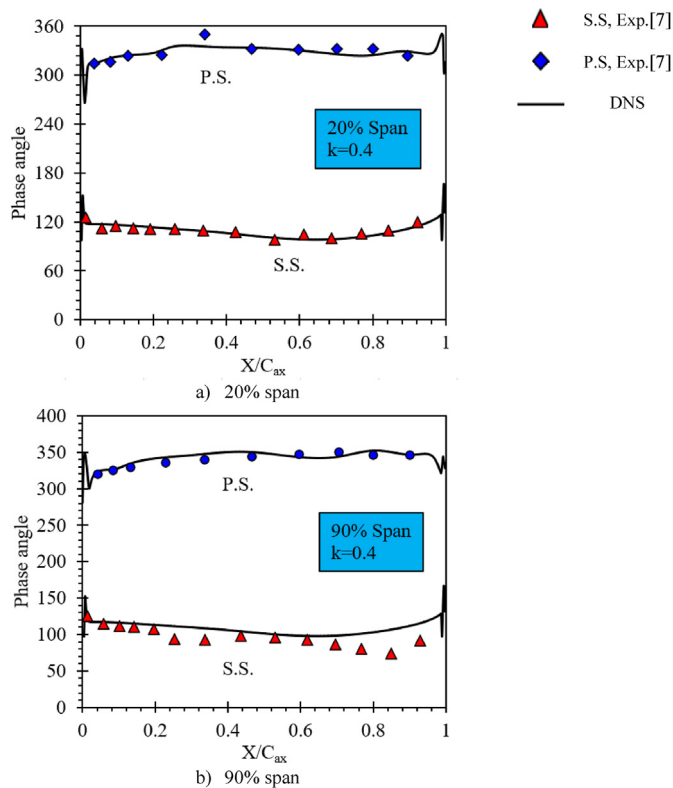


Fig. 9. Pressure phase angle over the vibrating compressor cascade ( $k = 0.4$ ) at two different span sections.

experiment. The difference in variation of the phase angle between the pressure and suction surfaces of the blade is greater at 90% span as the phase angle deviates between  $120^\circ$  and  $300^\circ$  at 20% span, whereas it varies between  $100^\circ$  and  $350^\circ$  at 90% span. A close agreement between the DNS simulation and the experiment was obtained with all sections of the blade, indicating that the present numerical model accurately captured and predicted unsteady pressure distributions over the blade surfaces.

The instantaneous pressure contours and streamlines obtained from the stationary and the vibrating compressor blades are illustrated in Fig. 10 to highlight the effects of the blade vibrations on the pressure variations in the computational domain. In both cases, pressure bubbles and flow recirculation are created on the suction side within the separation zone. The blade vibration further amplifies the flow instability and the production of pressure bubbles. It is observed that strong pressure bubbles are developed on the suction side due to the blade oscillation, which later leads to flow recirculation. These observations clearly indicate that the blade vibration and motion influence the pressure fluctuation and distribution around the blade of a compressor cascade.

The blade motion not just affects the pressure distribution and vortex generation process but also influences the downstream wake. Fig. 11 presents the axial velocity distributions from both stationary and oscillating blades. The effect of vibration frequency using two reduced frequencies, 0.2 and 0.4, are also investigated in this paper. In all cases, the flow separates from the suction side, and the separation bubbles and the vortex structures shed away from the trailing edge. At  $k = 0.2$ , the downstream flow is comparable to that of the stationary blade; however, stronger separation bubbles can be observed in the separation region on the suction side. A significant difference between the vibrating blade and stationary blade cases can be seen at  $k = 0.4$ . A higher blade vibration frequency triggers additional flow disturbance causing the larger flow separation and the stronger vortex generation. It is also clearly observed that the downstream wake is highly distorted by the flow disturbances introduced by the blade vibration. Fig. 12 shows the downstream wake profile extracted from the stationary and the vibrating blades at the reduced frequency of 0.4. The experiment results for the stationary blade are also added to the comparison. It is observed that the results from the DNS analysis using the stationary blade are in excellent agreement with the experiment [32]. In the case of the blade vibration, the magnitude of the wake profile is comparable to that of the stationary blade. However, strong fluctuations are observed at the centre of the wake. These fluctuations are activated by the flow disturbances resulting from the blade oscillation. Therefore, it can be said that the blade oscillations have a substantial effect on different aspects of unsteady flow behaviour, including flow separation, vortex generation and formation of the downstream wake.

The vorticity isosurface over the stationary and oscillating blades are demonstrated in Fig. 13. The impact of the blade motion on the development of vortex flow is highlighted. As the flow passes through the blade, it is mainly attached to the pressure side and somewhat attached to the suction side until it starts separating. The separation point is different in the two cases, as discussed in Fig. 7. In the case of the vibrating blade, the flow starts to recirculate as soon as it separates, and it becomes stronger as it moves towards the trailing edge, where the flow turns fully turbulent. The formations of dynamic stall vortex structures are also seen near the trailing edge, which adds flow disturbances to the downstream wake. In contrast to the stationary blade, the vorticity structures are larger, and the downstream flow is sharper in the vibrating blade.

Power spectral density (PSD) of the instantaneous pressure signals is calculated at the specific point in the compressor blade wake region in Fig. 14. The measuring point is selected at the mid-

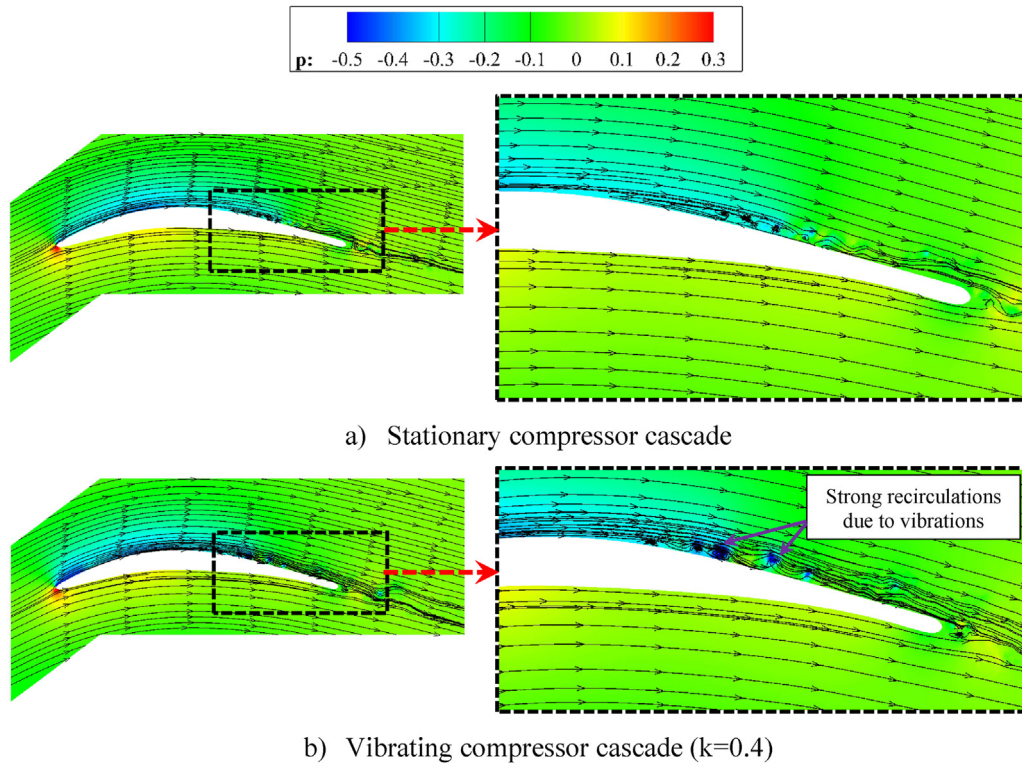


Fig. 10. Pressure contours and velocity streamlines over the stationary and vibrating compressor blade cascade at 50% span.

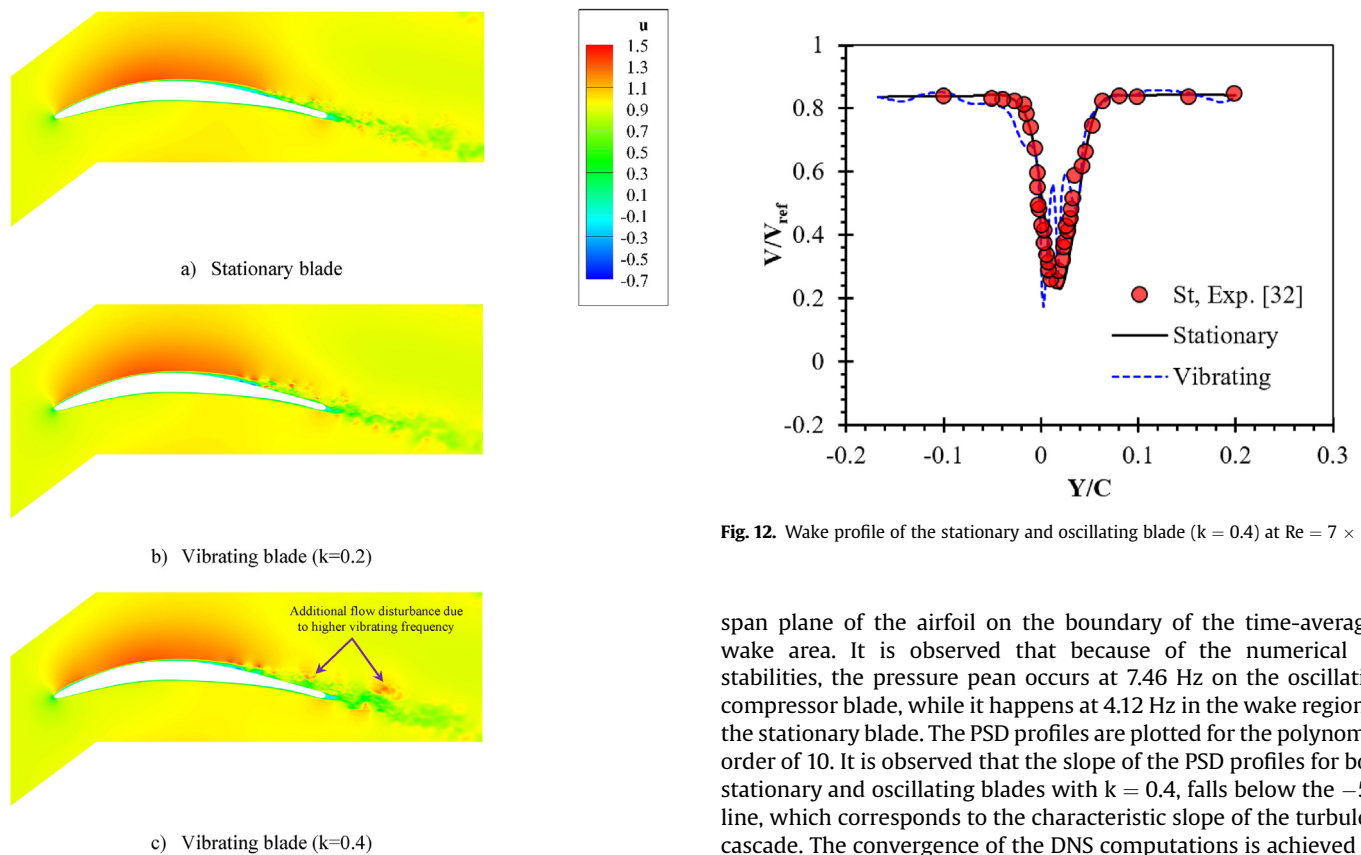
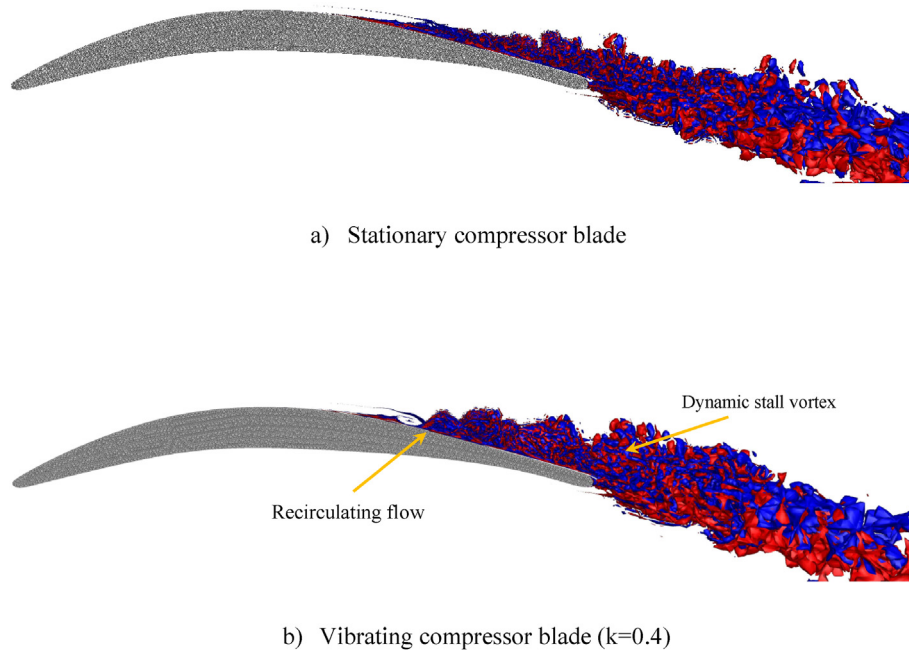
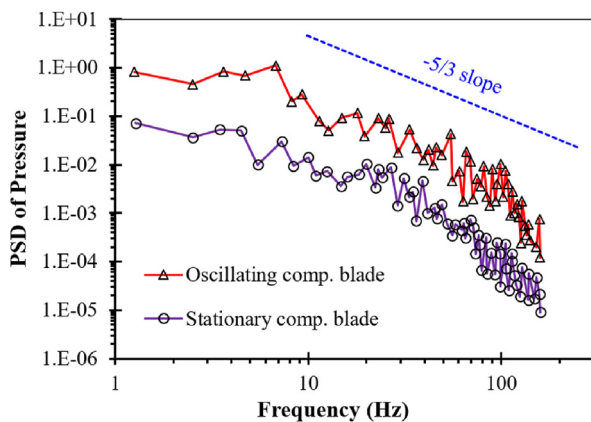


Fig. 11. Axial velocity contours over the stationary and vibrating linear compressor cascade.

span plane of the airfoil on the boundary of the time-averaged wake area. It is observed that because of the numerical instabilities, the pressure peak occurs at 7.46 Hz on the oscillating compressor blade, while it happens at 4.12 Hz in the wake region of the stationary blade. The PSD profiles are plotted for the polynomial order of 10. It is observed that the slope of the PSD profiles for both stationary and oscillating blades with  $k = 0.4$ , falls below the  $-5/3$  line, which corresponds to the characteristic slope of the turbulent cascade. The convergence of the DNS computations is achieved for all tested stationary and vibrating compressor blades in the gas turbine.



**Fig. 13.** Vorticity isosurface contours over the stationary and vibrating compressor blade for  $W_2 = \pm 20$  (+20: blue colour, -20: red colour). (For interpretation of the references to colour in this figure legend, the reader is referred to the Web version of this article.)



**Fig. 14.** PSD of pressure signals over the stationary and vibrating ( $k = 0.4$ ) compressor blade cascade.

### 5. Conclusion

In this paper, high-fidelity DNS simulations are performed on a compressor cascade blade. Developing high-fidelity transient models is necessary to investigate the flow structure and instantaneous bubble formation over the turbine blades. The effect of the blade oscillation on the aeroelasticity and the transitional flow structures are thoroughly analysed in comparison to the stationary blade. The results from the present DNS simulations are compared to the experiment, and an excellent agreement is obtained between the two methods.

The overall conclusions drawn based on the evaluated results of this paper are:

- The behaviour of the unsteady flow, including the flow separation, the vortex generation and the formation of the downstream wake, are all strongly influenced by the blade oscillation.

- The flow separation point is affected by the blade motion, and it also depends on the vibration characteristics such as vibration frequency and amplitude. The flow separation bubbles are magnified by the oscillatory motion of the blade that leads to a stronger vortex generation and additional flow disturbances.
- The separation point occurred 8.28% sooner on the suction surface of the vibrating blade with  $k = 0.4$  ( $X_{sep}/C = 0.288$ ) compared to the stationary blade with  $X_{sep}/C = 0.314$ .
- The harmonic oscillations of the blade amplify the flow disturbances, contributing to the trailing edge vortex shedding adding more turbulence to the downstream wake. The vortex structures are also larger in the vibrating blade case.
- The difference in variation of the phase angle between the pressure and suction surfaces of the blade is greater at 90% span as the phase angle deviates between  $120^\circ$  and  $300^\circ$  at 20% span, whereas it varies between  $100^\circ$  and  $350^\circ$  at 90% span.

### Credit author statement

**Mahdi Erfanian Nakhchi:** Conceptualization, Methodology, Software, Formal analysis, Visualization, Writing – original draft. **Shine Win Naung:** Writing – review & editing, Validation, Investigation. **Mohammad Rahmati:** Conceptualization, Methodology, Writing– review & editing, Funding acquisition, Supervision.

### Data availability statement

All research data supporting this publication are directly available within this publication.

### Declaration of competing interest

The authors declare that they have no known competing financial interests or personal relationships that could have appeared to influence the work reported in this paper.

## Acknowledgements

The authors would like to acknowledge the financial support received from the Engineering Physics and Science Research Council of the UK (EPSRC EP/R010633/1).

## References

- [1] Ibrahim TK, Mohammed MK, Al Door WHA, Al-Sammarrate AT, Basrawi F. Study of the performance of the gas turbine power plants from the simple to complex cycle: a technical review. *J. Adv. Res. Fluid Mech. Thermal Sci.* 2019;57:228–50.
- [2] Ibrahim TK, Basrawi F, Awad OI, Abdullah AN, Najafi G, Mamat R, Hagos F. Thermal performance of gas turbine power plant based on exergy analysis. *Appl Therm Eng* 2017;115:977–85.
- [3] Ibrahim TK, Rahman M, Mohammed M, Basrawi F. Statistical analysis and optimum performance of the gas turbine power plant. *Int J Automot Mech Eng* 2016;13:3215.
- [4] Brahimi F, Ouibrahim A. Blade dynamical response based on aeroelastic analysis of fluid structure interaction in turbomachinery. *Energy* 2016;115:986–95.
- [5] Naung SW, Nakhchi ME, Rahmati M. Prediction of flutter effects on transient flow structure and aeroelasticity of low-pressure turbine cascade using direct numerical simulations. *Aero Sci Technol* 2021;119:107151.
- [6] Li H, Ekici K. A novel approach for flutter prediction of pitch–plunge airfoils using an efficient one-shot method. *J Fluid Struct* 2018;82:651–71.
- [7] Yang H, He L. Experimental study on linear compressor cascade with three-dimensional blade oscillation. *J Propul Power* 2004;20:180–8.
- [8] Rahmati M, He L, Wang D, Li Y, Wells R, Krishnababu S. Non-linear time and frequency domain methods for multi-row aeromechanical analysis. *Turbo Expo: power for Land, Sea, and Air. Am Soc Mech Eng* 2012:1473–85.
- [9] Win Naung S, Rahmati M, Farokhi H. Aerodynamic analysis of a wind turbine with elevated inflow turbulence and wake using harmonic method, international conference on offshore mechanics and arctic engineering. *Proceedings of the ASME 2019 38th International Conference on Ocean, Offshore and Arctic Engineering*. Volume 10: Ocean Renewable Energy. Glasgow, Scotland, UK. June 9–14, 2019:V010T009A062. <https://doi.org/10.1115/OMAE2019-96769>.
- [10] Win Naung S, Rahmati M, Farokhi H. Aeromechanical analysis of wind turbines using non-linear harmonic method, international conference on offshore mechanics and arctic engineering. *Proceedings of the ASME 2019 38th International Conference on Ocean, Offshore and Arctic Engineering*. Volume 10: Ocean Renewable Energy. Glasgow, Scotland, UK. June 9–14, 2019:V010T009A060. <https://doi.org/10.1115/OMAE2019-96256>.
- [11] Wang X, Zou Z. Uncertainty analysis of impact of geometric variations on turbine blade performance. *Energy* 2019;176:67–80.
- [12] Du J, Li Y, Li Z, Li J, Wang Z, Zhang H. Performance enhancement of industrial high loaded gas compressor using Coanda jet flap. *Energy* 2019;172:618–29.
- [13] Yonezawa K, Nakai G, Takayasu M, Sugiyama K, Sugita K, Umezawa S, Ohmori S. Influence of blade corrosion on aerodynamic characteristics of a gas turbine. *Energy* 2021;230:120665.
- [14] Shuai J, Jianyang Y, Hongwu W, Fu C, Shaowen C, Yanping S. Experimental investigation of the bending clearance on the aerodynamic performance in turbine blade tip region. *Energy* 2020;197:117234.
- [15] Moussavi SA, Benisi AH, Durali M. Effect of splitter leading edge location on performance of an automotive turbocharger compressor. *Energy* 2017;123:511–20.
- [16] Zhang Y, Deng S, Wang X. RANS and DDES simulations of a horizontal-axis wind turbine under stalled flow condition using OpenFOAM. *Energy* 2019;167:1155–63.
- [17] Li Z, Liu Y. Blade-end treatment for axial compressors based on optimization method. *Energy* 2017;126:217–30.
- [18] Alam M, Sandham ND. Direct numerical simulation of short-laminar separation bubbles with turbulent reattachment. *J Fluid Mech* 2000;410:1–28.
- [19] Vahdati M, Simpson G, Imregun M. Mechanisms for wide-chord fan blade flutter. *J Turbomach* 2011;133.
- [20] Naung SW, Rahmati M, Farokhi H. Direct numerical simulation of interaction between transient flow and blade structure in a modern low-pressure turbine. *Int J Mech Sci* 2020;192:106104.
- [21] Nakhchi M, Rahmati M. Direct numerical simulations of flutter instabilities over a vibrating turbine blade cascade. *J Fluid Struct* 2021;104:103324.
- [22] Moriguchi S, Miyazawa H, Furusawa T, Yamamoto S. Large eddy simulation of a linear turbine cascade with a trailing edge cutback. *Energy* 2021;220:119694.
- [23] Nakhchi M, Naung SW, Rahmati M. High-resolution direct numerical simulations of flow structure and aerodynamic performance of wind turbine airfoil at wide range of Reynolds numbers. *Energy* 2021;225:120261.
- [24] D'Alessandro V, Clementi G, Giannichele L, Ricci R. Assessment of the dimples as passive boundary layer control technique for laminar airfoils operating at wind turbine blades root region typical Reynolds numbers. *Energy* 2019;170:102–11.
- [25] G. Karniadakis, S. Sherwin, *Spectral/hp element methods for computational fluid dynamics*, Oxford University Press 2013.
- [26] Sherwin SJ, Ainsworth M. Unsteady Navier–Stokes solvers using hybrid spectral/hp element methods. *Appl Numer Math* 2000;33:357–63.
- [27] Cantwell CD, Moxey D, Comerford A, Bolis A, Rocco G, Mengaldo G, De Grazia D, Yakovlev S, Lombard J-E, Ekelschot D, Nektar++: an open-source spectral/hp element framework. *Comput Phys Commun* 2015;192:205–19.
- [28] Yan Z-G, Pan Y, Castiglioni G, Hillewaert K, Peiró J, Moxey D, Sherwin SJ. Nektar++: design and implementation of an implicit, spectral/hp element, compressible flow solver using a Jacobian-free Newton Krylov approach. *Comput Math Appl* 2021;81:351–72.
- [29] Moxey D, Cantwell CD, Bao Y, Cassinelli A, Castiglioni G, Chun S, Juda E, Kazemi E, Lackhove K, Marcon J, Nektar++. Enhancing the capability and application of high-fidelity spectral/hp element methods. *Comput Phys Commun* 2020;249:107110.
- [30] Bao Y, Palacios R, Graham M, Sherwin S. Generalized thick strip modelling for vortex-induced vibration of long flexible cylinders. *J Comput Phys* 2016;321:1079–97.
- [31] Cassinelli A, Adami P, Montomoli F, Sherwin SJ. On the effect of wake passing on a low pressure turbine cascade using spectral/textit {hp} element methods. *Bull Am Phys Soc* 2019:64.
- [32] Elazar Y, Shreeve R. Viscous flow in a controlled diffusion compressor cascade with increasing incidence. 1990.
- [33] Nakhchi ME, Naung SW, Rahmati M. DNS of secondary flows over oscillating low-pressure turbine using spectral/hp element method. *Int J Heat Fluid Flow* 2020;86:108684.
- [34] Vos PE, Sherwin SJ, Kirby RM. From h to p efficiently: implementing finite and spectral/hp element methods to achieve optimal performance for low- and high-order discretisations. *J Comput Phys* 2010;229:5161–81.
- [35] Dong S, Karniadakis GE, Chrysostomidis C. A robust and accurate outflow boundary condition for incompressible flow simulations on severely-truncated unbounded domains. *J Comput Phys* 2014;261:83–105.
- [36] Cassinelli A, Xu H, Montomoli F, Adami P, Vazquez Diaz R, Sherwin SJ. On the effect of inflow disturbances on the flow past a linear LPT vane using spectral/hp element methods. *Turbo Expo: power for Land, Sea, and Air. American Society of Mechanical Engineers*; 2019. V02CT41A032.